Aharonov-Bohm effect for an exciton in a finite-width nanoring

F. Palmero*

Grupo de Física No Lineal, Departamento de Física Aplicada I, ETSI Informática, Universidad de Sevilla, Avd. Reina Mercedes s/n, 41012-Sevilla, Spain

J. Dorignac[†] and J. C. Eilbeck

Department of Mathematics, Heriot-Watt University, Riccarton, Edinburgh, EH14 4AS, United Kingdom

R. A. Römer

Department of Physics and Centre for Scientific Computing, University of Warwick, Coventry, CV4 7AL, United Kingdom

We study the Aharonov-Bohm effect for an exciton on a nanoring using a 2D attractive fermionic Hubbard model. We extend previous results obtained for a 1D ring, in which only azimuthal motion is considered, to a more general case of 2D annular lattices. In general, we show that the existence of the localization effect, increased by the nonlinearity, makes the phenomenon in the 2D system similar to the 1D case. However, the introduction of radial motion introduces extra frequencies, different from the original isolated frequency corresponding to the excitonic Aharonov-Bohm oscillations. If the circumference of the system becomes large enough, the Aharonov-Bohm effect is suppressed.

PACS number(s): 71.35.−y, 63.20.Pw, 63.20.Ry

I. INTRODUCTION

Progress in microstructuring technology allows the construction of nanosized InGaAs rings by self-assembly[1–3] or using lithographic techniques.[4,5] Similarly, PbSe-based nanorectangles have been synthesized in solution through oriented attachment of nanocrystal building blocks.[6] In these systems, electrons and holes can propagate coherently and the existence of bound states—so-called excitons—offers an opportunity to explore the Aharonov-Bohm (AB) effect.[7,8] The exciton, although neutral, can be sensitive to a magnetic flux due to its finite-sized Bohr radius.[9] This effect, in the framework of excitons in nanorings, has been studied previously by means of simple models, such as a continuous one-dimensional (1D) quantum ring[9–13] or in continuous two-dimensional (2D) models for which some numerical solutions can be found.[14] The effects of an additional external electric field have also been studied.[15] In all cases, it has been shown that AB oscillations can exist in a finite-width nanoring, but when the ring becomes large enough, the effect is suppressed. A similar effect has also been predicted for bi-excitons.[13]

In this paper we consider lattice models of such nanorings with an electron and hole subject to a perpendicular and uniform magnetic flux. Our models allow for a finite number of transport channels, either arranged annularly, i.e., coupled rings laid out in a 2D plane with increasing radius, or stacked vertically. Therefore, we can study in a controlled way how the excitonic AB oscillations evolve when additional rings are added, either in-plane or vertically. We describe the electron-hole system on the rings by means of an attractive Hubbard model where electron and hole are modeled as spin-up and spin-down particles with different effective masses. We focus our interest on the study of the AB oscillations, their dependence on the size of the rings, and on different combinations of lattice parameters.

For attractive Hubbard models, the existence of bound states of electrons and holes—identical to spin-singlets when using the standard electronic interpretation—is well known,[16] and has previously also been studied in the framework of quantum breathers.[17] In these cases, if the anharmonicity (interaction strength) is strong enough, there is an extended Bloch state with two or more particles in a strongly correlated state. There exist various theoretical[18–20] and numerical[21] results as well as experimental observations of these states in different quantum systems.[22–24]

Our work is organized as follows: in the next section we present the model. In Sec. III we study the 1D model and analytical expressions are obtained and compared to the 1D continuum approach. In Sec. IV, we consider a simple *plate-shaped* two-ring model and compare the AB oscillations with those obtained in the 1D case. In Sec. V, we extend our results to a finite number (>2) of rings. In Sec. VI, we consider a model in which the rings have been stacked vertically, so that the same flux is threading each ring. Finally, in Sec. VII, we summarize our findings and present our conclusions.

II. THE MODEL

We consider an anharmonic 2D lattice of N rings, each ring with M sites, subject to a uniform magnetic field perpendicular to the lattice, as shown in Fig. 1. On this lattice we consider an electron and a hole. We assume that the interaction potential is short ranged and the system can be described by an attractive fermionic Hubbard model. Also, we will consider only the possibility of hopping between nearest-neighbor sites. Thus, the Hamiltonian is given by
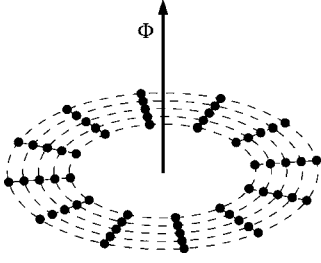
FIG. 1. Sketch of the model. The lattice is a 2D system of N rings and M sites in each ring. The system is subject to a uniform magnetic field perpendicular to the lattice, with Φ the magnetic flux.

$$
\hat{H} = -\gamma \sum_{n=1}^{N} \sum_{m=1}^{M} a_{n,m}^{\dagger} a_{n,m} b_{n,m}^{\dagger} b_{n,m} - \sum_{n=1}^{N-1} \sum_{m=1}^{M} t_n^{\perp} [a_{n,m}^{\dagger} a_{n+1,m}
$$
$$
+ a_{n+1,m}^{\dagger} a_{n,m} + \mu(b_{n,m}^{\dagger} b_{n+1,m} + b_{n+1,m}^{\dagger} b_{n,m})]
$$
$$
- \sum_{n=1}^{N} \sum_{m=1}^{M} t_n^{\parallel} [e^{2\pi i \varphi_n/M}(a_{n,m}^{\dagger} a_{n,m+1} + \mu b_{n,m+1}^{\dagger} b_{n,m})
$$
$$
+ e^{-2\pi i \varphi_n/M}(a_{n,m+1}^{\dagger} a_{n,m} + \mu b_{n,m}^{\dagger} b_{n,m+1})]. \tag{1}
$$

Here $a_{n,m}^{\dagger}(a_{n,m})$ and $b_{n,m}^{\dagger}(b_{n,m})$ are raising (lowering) operators for electrons and holes, respectively, satisfying the standard fermionic anticommutation relations. The parameters $t_n^{\parallel}$ represent the hopping coefficient between neighboring sites along the nth ring, and $t_n^{\perp}$ the hopping coefficients between neighboring sites, one corresponding to the nth ring and the other one to the $(n+1)$th ring (in the absence of magnetic field). In general, these coefficients will depend on the distance between sites. For an annular ring structure as in Fig. 1, the site-to-site distances increase as one moves further away from the center. In a single ring with no interaction ($\gamma=0$), the effective mass of the electron and hole at the extrema of the conduction and valence band are proportional

to the inverse of the square of the distance between sites [12]. In our model, we have chosen, for a fixed value value of the number of sites, a fixed effective mass for all the rings with different radius and, therefore, we model the intraring nearest-neighbor hopping coefficient by assuming a dependence according to an inverse-square law. Also, we consider a similar dependence for the interring hopping coefficient. Thus,

$$
t_n^{\perp} = \frac{\epsilon}{(r_{n+1} - r_n)^2}, \quad t_n^{\parallel} = \frac{\epsilon}{4 r_n^2 \sin^2(\pi/M)}, \tag{2}
$$

where r_n is the radius of the nth ring and $d_n = 2 r_n \sin(\pi/M)$ is the chord distance between two neighboring lattice points of the nth ring. Also, the formal continuum limit can be obtained by taking this distance going to zero. We will suppose that the distance between rings is constant, $t_n^{\perp} = t^{\perp}$, and thus independent of the ring. The parameter γ/ϵ represents the ratios of anharmonicity (interaction parameter) to nearest-neighbor hopping energy, μ the ratio of the effective masses of electrons and holes at the bottom and the top of the conduction and valence band respectively, and $\varphi_n = \Phi_n/\Phi_0$, Φ_n the magnetic flux through the nth ring and Φ_0 the flux quantum. In general we consider $\epsilon = 1$ and $\mu = 0.2$, as in Ref. 14.

The 1D Hubbard model with nearest-neighbor hopping terms has been solved exactly in the seminal papers by Lieb and Wu[16] and with flux by Shastry and Sutherland.[26,27] Recent results are reviewed in Ref. 28. Similarly exact results for extensions of the model are rare. An approximation to calculate the spectrum of the Hubbard model has been proposed (see, e.g., Ref. 25, where the exact spectrum and thermodynamics for a long-range hopping Hubbard chain with linear dispersion is calculated). In this paper, we will use the number-state method[17] to calculate the eigenvalues and eigenvectors of the Hamiltonian operator (1) in the sector with a single electron and a single hole. We use a number-state basis

$$
|\psi_{\{n\}}\rangle = \left| \begin{matrix} n_1^e, n_2^e, \ldots, n_M^e; n_{M+1}^e, n_{M+2}^e, \ldots, n_{2M}^e; n_{M+1}^e, \ldots \ldots; n_{M(N-1)+1}^e, n_{M(N-1)+2}^e, \ldots, n_{MN}^e \\ n_1^h, n_2^h, \ldots, n_M^h, n_{M+1}^h, n_{M+2}^h, \ldots, n_{2M}^h; n_{M+1}^h, \ldots \ldots; n_{M(N-1)+1}^h, n_{M(N-1)+2}^h, \ldots, n_{MN}^h \end{matrix} \right\rangle, \tag{3}
$$

where $n_{(m-1)N+n}^e(n_{(m-1)N+n}^h)$ represents the numbers of electrons (holes) at site n of the ring m. We always have $\Sigma_{n,m} n_{(m-1)N+n}^e = 1$ and $\Sigma_{n,m} n_{(m-1)N+n}^h = 1$. A general wave function is $|\Psi\rangle = \Sigma_{\{n\}} c_{\{n\}} |\psi_{\{n\}}\rangle$. It is possible to block diagonalize the Hamiltonian operator using eigenfunctions of the periodic translation (or rotation) operator $\hat{T}$ defined as $\hat{T} b_{n,m}^{\dagger} = b_{n,m+1}^{\dagger} \hat{T}$ ($\hat{T} a_{n,m}^{\dagger} = a_{n,m+1}^{\dagger} \hat{T}$). In each block, the eigenfunctions have a fixed value of the *total* momentum K, with $\tau = \exp(iK)$ being an eigenvalue of $\hat{T}$ such that $K = 2\ell\pi/M$ and ℓ integer.[17]

In general, if the anharmonicity parameter is large enough, there exists some isolated eigenvalue for each k which corresponds to a localized eigenfunction. By "localized," we mean there is a high probability for finding the two fermions at the same site. This is illustrated by the band structure in Fig. 2, which shows two isolated bands below the two "continuum" bands. Due to the rotational invariance of the system, there is the same probability of finding two fermions at any site of a ring. In these cases, analytical expressions can be obtained in some asymptotic limits.[17,18,29]
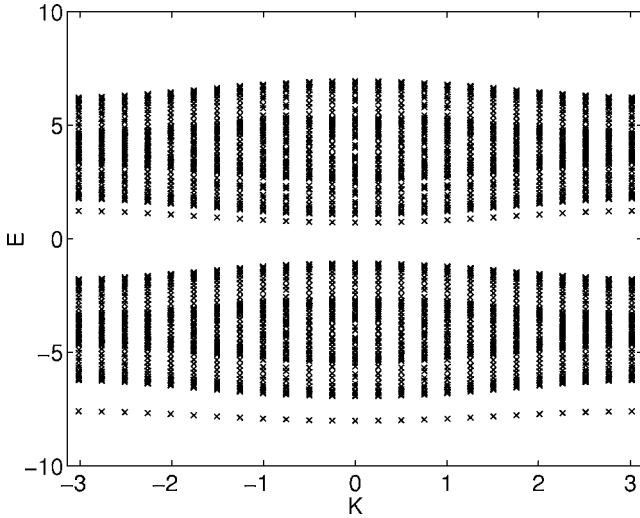
FIG. 2. Band structure of the eigenvalues $E(k)$. $M=25$, $N=2$, $\gamma=4$, $\varphi_1=\varphi_2=0$, $d_1=1$, $\epsilon=1$, $\mu=0.2$. $\Delta r=r_2-r_1=0.5$.

III. A SINGLE RING

A. The Hamiltonian matrix

In the simplest case, $N=1$, the system reduces to a 1D ring of M sites and radius r. The Hamiltonian matrix in each momentum subspace is given as

$$H_1^{(K)} = - \begin{bmatrix} \gamma & q^* & 0 & . & . & q \\ q & 0 & q^* & 0 & . & 0 \\ 0 & q & 0 & q^* & . & . \\ . & . & . & . & . & . \\ . & . & . & q & 0 & q^* \\ q^* & . & . & . & q & 0 \end{bmatrix}, \quad (4)$$

where $q=t^{\|}e^{2\pi i\varphi/M}(\mu+e^{-iK})$ and we have omitted the index labelling the ring number. In the case of no interaction ($\gamma=0$) between the electron and hole, the energy of the system is given by

$$E_{k^e,k^h} = -2t^{\|}\cos\left(k^e - \frac{2\pi\Phi}{M\Phi_0}\right) - 2t^{\|}\mu\cos\left(k^h + \frac{2\pi\Phi}{M\Phi_0}\right), \quad (5)$$

where $k^e,k^h=2\pi\ell/M$ are the *single particle* wave vectors in the absence of a magnetic field,[12] and $K=k^e+k^h$. In the continuous limit, when $M\to\infty$, $d\to0$ but the radius of the ring is fixed, and considering the energy of the ground state in the absence of the field for the electron and hole as zero, Eq. (5) reduces to the standard parabolic expressions for charges in a continuous ring threaded by a magnetic flux and no interaction.[9]

B. Exact results

For $\gamma\neq0$, the ground state in each momentum sector associated with Eq. (4) is given by[17]

$$|\Psi_\tau\rangle = c_0\sum_{j=1}^M (\hat{T}/\tau)^{j-1}\left|\begin{matrix}10\cdots0\\10\cdots0\end{matrix}\right\rangle \quad (6)$$

$$+ c_1\sum_{j=1}^M (\hat{T}/\tau)^{j-1}\left|\begin{matrix}10\cdots0\\01\cdots0\end{matrix}\right\rangle \quad (7)$$

$$+ \ldots + c_{M-1}\sum_{j=1}^M (\hat{T}/\tau)^{j-1}\left|\begin{matrix}10\cdots0\\00\cdots1\end{matrix}\right\rangle, \quad (8)$$

where

$$c_n = \frac{c_0 e^{in\theta}}{\sinh(M\nu)}\{\sinh[(M-n)\nu] + e^{-iM\theta}\sinh(n\nu)\}, \quad (9)$$

$\theta=\arg(q)$, $\cosh(\nu)=-E/2|q|$, and c_0 is a normalization factor. Details of the calculation can be found in Sec. 1 of the Appendix. The energy spectrum $E_\nu=-2|q|\cosh(\nu)$ is determined by the solutions of the equation

$$\frac{\tanh(M\nu)}{\sinh(\nu)} = \frac{2|q|}{\gamma}\left(1 - \frac{\cos(M\theta)}{\cosh(M\nu)}\right). \quad (10)$$

As we show in Sec. 2 of the Appendix, bound state solutions to Eq. (10) exist iff

$$\gamma > \frac{2|q|}{M}(1 - \cos M\theta). \quad (11)$$

These solutions correspond to the bound electron-hole pair, namely the *exciton*. In the limit $M\to\infty$, d constant, the energy of the exciton is $E_\infty=-\sqrt{\gamma^2+4|q|^2}$, independent of the value of the magnetic field. This value corresponds to the exciton binding energy in a straight wire.[9] Also, the anharmonic/interaction parameter γ must scale as $1/d$ in order to support a bound state solution; it goes to infinity as expected for a point-like δ-function interaction.[30]

C. Approximations for a large ring

If Md is large, we can derive some explicit approximate expressions (see Sec. 3 of the Appendix for details). First, the energy of the bound state is given by

$$E = E_\infty\left[1 + \frac{2\gamma^2}{E_\infty^2}\cos(M\theta)\exp^{-M\operatorname{arcsinh}(\gamma/2|q|)}\right]. \quad (12)$$

This formula is close to the perturbative exciton energy obtained for a large ring radius in the continuum model.[9] Also, if d is small enough, condition (11) can be approximated as $2\pi r\beta>1-\cos(2\pi\Phi/\Phi_0)$, where $\beta=\operatorname{arcsinh}(\gamma/2|q|)/d$ is the inverse decay length of energy oscillations given by Eq. (12).

D. Numerical results

In Fig. 3 we plot the energy of the ground state for several values of the magnetic flux and the circumference $\rho=2\pi r$ of the ring. It is easy to see that the magnitude of the AB effect decreases rapidly with increasing ring radius. As expected,[9] the maximum amplitude of the AB oscillations corresponds to integer or half-integer values of Φ/Φ_0. If we analyze the (unbound) excited states, the contributions of components corresponding to states where fermions are localized in different sites of the lattice are significant, and the AB contri-
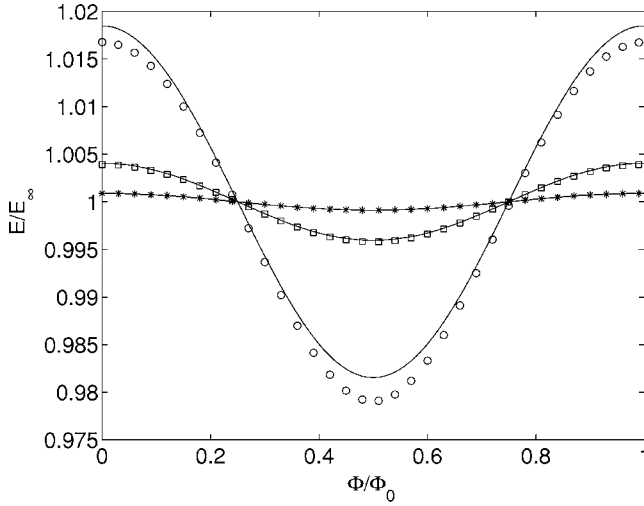
FIG. 3. The Aharonov-Bohm oscillations of exciton energy (in units of E_∞) corresponding to three values of the (single) ring circumference ρ (in units of d) obtained by solving Eq. (10) numerically for $\gamma=2$, $d=1$, $\epsilon=1$, $\mu=0.2$, and $k=0$. ($\bigcirc$) $M=5$ ($\rho=5.34$), ($\square$) $M=7$ ($\rho=7.24$), and ($*$)$M=9$ ($\rho=9.19$). The lines denote the approximate solutions given by Eq. (12).

bution no longer decreases exponentially with the circumference of the ring.

For the ground state, if we plot the amplitude of the AB oscillations $\Delta E=E(\varphi=0)-E(\varphi=1/4)$ as a function of circumference ρ as shown in Fig. 4, we observe an exponential decay with a decay length d_c which can be calculated numerically by solving Eq. (10). The characteristic decay length is a function of the anharmonic parameter γ and, as shown in Fig. 5, it decreases with increasing γ.
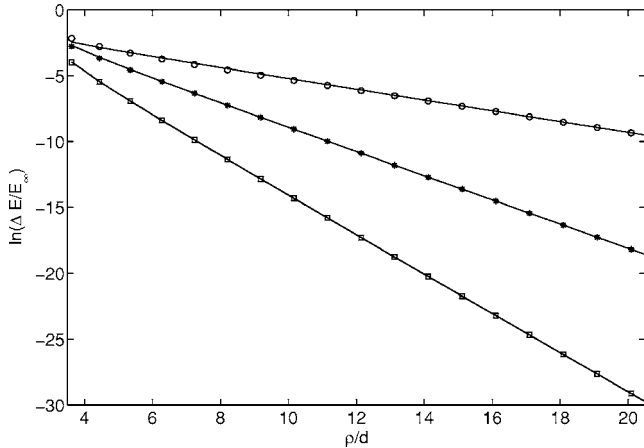

FIG. 4. Energy oscillations amplitude of AB oscillations (in units of E_∞ and on a semi–logarithm scale) as a function of the circumference of the (single) ring ρ (in units of circumferential lattice spacing d), obtained by solving Eq. (10) numerically for $\gamma=1$, corresponding to a weakly bounded state ($\bigcirc$), $\gamma=2.5$, a typical bound state ($*$), and $\gamma=5$, corresponding to a strongly bound state ($\square$). $\epsilon=1$, $\mu=0.2$, and $k=0$. The continuous lines are approximate solutions given by Eq. (12). All logarithms are natural logarithms.
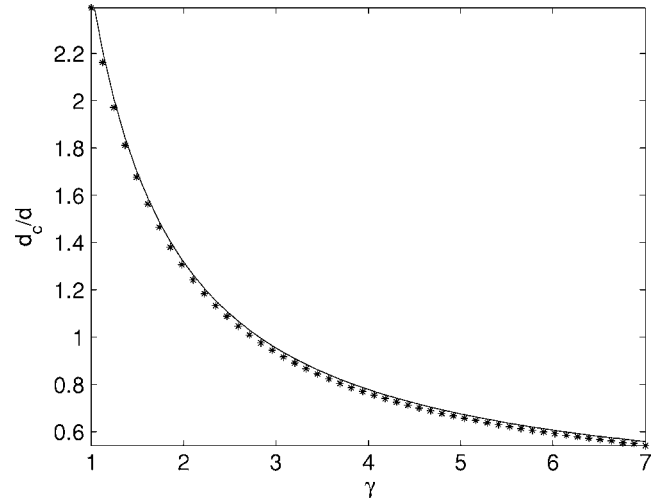

FIG. 5. Decay length d_c of AB oscillations (in units of the circumferential lattice spacing d) for a single ring as a function of the anharmonic parameter γ. $\epsilon=1$, $\mu=0.2$, and $k=0$, obtained by numerical solution of Eq. (10) ($*$). The continuous line is the approximate solution given by Eq. (12).

IV. THE CASE OF TWO RINGS

A. The Hamiltonian matrix

In the case of two rings ($N=2$) with M sites on each, it is again possible to find the Hamiltonian matrix $H^{(K)}$ in each total momentum K subspace,

$$H_2^{(K)} = - \begin{bmatrix} H_{11} & H_{12} & H_{13} & H_{14} \\ H_{12}^* & H_{22} & H_{23} & H_{13} \\ H_{13}^* & H_{23}^* & H_{33} & H_{12} \\ H_{14}^* & H_{13}^* & H_{12}^* & H_{44}, \end{bmatrix}, \quad (13)$$

where each H_{ij} submatrix is of dimension $M \times M$. The diagonal blocks are given by $H_{11}=\mathcal{F}(\gamma,q_1)$, $H_{44}=\mathcal{F}(\gamma,q_2)$, $H_{22}=\mathcal{F}(0,q_{12})$, and $H_{33}=\mathcal{F}(0,q_{21})$ with the $M \times M$ matrix $\mathcal{F}(p,q)$ given by

$$\mathcal{F}(p,q) = \begin{bmatrix} p & q^* & 0 & . & . & q \\ q & 0 & q^* & 0 & . & 0 \\ 0 & q & 0 & q^* & . & . \\ . & . & . & . & . & . \\ . & . & . & q & 0 & q^* \\ q^* & . & . & . & q & 0 \end{bmatrix}. \quad (14)$$

The off-diagonal blocks are $H_{12}=\mu t_1^\perp \mathbb{1}$, $H_{13}=t_1^\perp \mathbb{1}$, where $\mathbb{1}$ is a $M \times M$ unit matrix, and the parameters are

$$q_1 = t_1^\| e^{2\pi i \varphi_1/M}(\mu + e^{-iK}), \quad (15)$$

$$q_2 = t_2^\| e^{2\pi i \varphi_2/M}(\mu + e^{-iK}), \quad (16)$$

$$q_{12} = t_1^\| e^{2\pi i \varphi_1/M}e^{-iK} + t_2^\| e^{2\pi i \varphi_2/M}\mu, \quad (17)$$
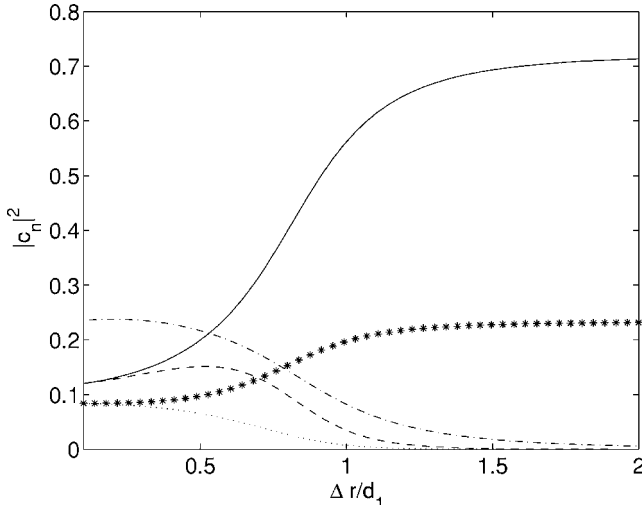
FIG. 6. Main components of the wave function corresponding to the ground state as a function of the distance between rings Δr (in units of inner ring circumferential lattice spacing d_1). $\gamma=2.5$, $\epsilon=1$, $\mu=0.2$, $M=15$, and $N=2$. (—) two fermions in a bound state on the inner ring, (---) two fermions in a bound state on the outer ring, (·–) two fermions in a nonbound state in contiguous sites and different rings, (*) two fermions in a nonbound state in contiguous sites and on the inner ring, and (···) two fermions in a nonbound state in contiguous sites and on the outer ring.

$$q_{21} = t_2^{\parallel} e^{2\pi i \varphi_2/M} e^{-iK} + t_1^{\parallel} e^{2\pi i \varphi_1/M} \mu. \qquad (18)$$

Other submatrices are null. Clearly, if $t_1^{\perp}=0$ and $r_1=r_2$, the system reduces to the 1D case studied before.

If Δr is small enough, the dominant elements of (13) are H_{12} and H_{13} and standard perturbation theory can be applied. In first-order approximation, the spectrum of $H_2^{(K)}$ is given by the superimposition of four subspectra. These subspectra are given by the spectrum of $-\mathcal{F}(2\gamma, Q)/4$ shifted by four different values: $(1+\mu)t_1^{\perp}$, $(1-\mu)t_1^{\perp}$, $(\mu-1)t_1^{\perp}$, and $(-1-\mu)t_1^{\perp}$, where $Q=q_1+q_2+q_{12}+q_{21}$. According to this result, we expect four bound states to exist but some of them can be hidden within the continuum bands, as shown in Fig. 2 where just two of them appear. Numerical tests confirm that this first-order perturbation result provides the right width for the continuum bands, but fails to precisely locate the bound states outside these bands. It also explains the intraband pattern observable in Fig. 2 in terms of overlapping bands of contiguous subspectra.

In the general case, it has not been possible to find an analytical expression for the eigenvectors and eigenvalues of Eq. (13), but they can be calculated numerically for different values of the control parameters and even large values of the number of sites M. In a similar way as in the previous section, we define E_{∞} as the energy of the ground state when $M \rightarrow \infty$ and $B=0$. This quantity is a function of the distance between both rings and its value can be determined numerically.

B. Fast and slow AB oscillations

In general, for strong attraction $\gamma>1$, as shown in Fig. 6,

the ground state is mainly a bound state, where fermions are located together in the same location and on the same ring. But in contrast to the 1D ring, we also find a contribution of components corresponding to states where fermions are in contiguous sites and on *different* rings as shown in Fig. 6. Thus, the variation of the ground state energy with Φ/Φ_0 consists of a combination of periodic functions with different frequencies. We find that the main contribution to the AB oscillations corresponds to the components where the fermions are located around the inner ring, with period Φ_1/Φ_0. There exists also a further oscillation corresponding to the contribution of the components where fermions are located around the outer ring, with period Φ_2/Φ_1. Due to the difference between hopping coefficients, a localization effect around the inner ring takes place, and, as shown in Ref. 31, this effect is enhanced by the nonlinearity. Thus, only when the distance between rings is very small, the contribution of the periodic term with period Φ_2/Φ_1 is (numerically) observable. In all cases, as in a 1D ring, the contribution of these terms to the energy oscillations with the magnetic flux decreases with the circumference of the ring.

There exists also a significant oscillation term coming from the contribution of nonlocalized states, where the electron and the hole are in contiguous sites but on different rings. These oscillations persist when the circumference of the ring increases, although their period increases, too. We will refer to this contribution as long-period oscillations. Essentially, the main period of these oscillations is given by the phase difference between the magnetic field term contribution in each ring. Assuming that $\gamma=0$ and using Eq. (5), this period is given by $T=2M/(\Phi_2/\Phi_1-1)=2M/(r_2/r_1-1)=2Mr_1/\Delta r$. The amplitude of the long-period oscillations decreases when the distance between the rings decreases. In cases where these oscillations are dominant, corresponding to cases where the distance between rings is small (or equivalently there is a large hopping coefficients $t^{\perp}$ between rings), the oscillations coming from components located around the same ring can be seen as a small modulation that decreases with the circumference of the ring. We note that a model in which the hole is located more towards the center of the ring has been put forward[32] in the context of the self-assembled nanorings.[1]

In general, if the distance between the rings is small, the ground state gives AB oscillations with period Φ_1/Φ_0. The first excited state, where the main components corresponding to the exciton are localized around the outer ring, oscillates with period Φ_2/Φ_0. If the distance between the rings is decreased, the hopping probability between different rings increases and the bands overlap. Then an additional oscillation of the energy appears due to the nonlocalized components in different rings.

C. Flux dependence

In Fig. 7 we show the flux dependence of the ground state energy for three different values of distance Δr and two different values of the circumference of the ring. In the top figure we can see the small AB oscillations, corresponding to the existence of the exciton state localized mainly around the
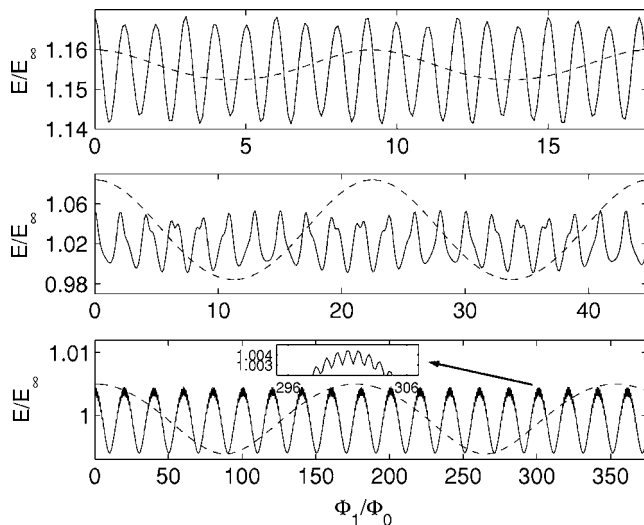
FIG. 7. Ground state energy oscillations of the exciton energy (in units of E_∞) as a function of Φ_1/Φ_0 for several values of the distance between different rings $\Delta r = r_2 - r_1$ (in units of the circumferential lattice spacing d_1) and different values of the circumference of the inner ring ρ_1. $\gamma = 2.5$, $\epsilon = 1$, $\mu = 0.2$, and $N = 2$. $\Delta r = 1.5$ (top), $\Delta r = 0.7$ (center), and $\Delta r = 0.1$ (bottom). Continuous lines correspond to $M = 5$ ($\rho_1 \sim 5.34$) and dashed lines to $M = 15$ ($\rho_1 \sim 15.11$).

inner ring. If the circumference is small enough, the AB oscillations are thus similar to the 1D case. If the circumference is larger, the amplitude of the AB oscillations decreases and the long-period oscillations become dominant. If the distance between the rings is similar to the distance between neighboring sites and the circumference of the rings is still small enough as shown in the central panel of Fig. 7, the excitonic AB oscillations are completely mixed-in with the the oscillations of similar frequencies coming from non-bound components in different rings. The bottom figure corresponds to the case where the two rings are close to each other. If the circumference is small enough, the excitonic AB oscillations appear as a slight modulation of the nonexcitonic oscillation due to the nonbound components in different rings. If the circumference is large enough, only the slow oscillations can be seen.

D. Fourier analysis of AB oscillations

If we analyze the Fourier spectrum of the oscillations of ground state energy as a function of magnetic flux in cases where the AB oscillations are not negligible (e.g., small M), and there are different values of distance between rings Δr, as shown in Fig. 8, we clearly detect the frequencies corresponding to AB oscillations in the inner ring and the oscillations due to nonlocalized components in different rings. A frequency corresponding to the contribution of components around the outer ring can only be seen if the distance between rings is very small ($\Delta r \simeq 0.1 d_1$).

E. Increasing the ring separation

If we study the decay of the amplitude ΔE of the ground state energy oscillations as a function of the distance be-
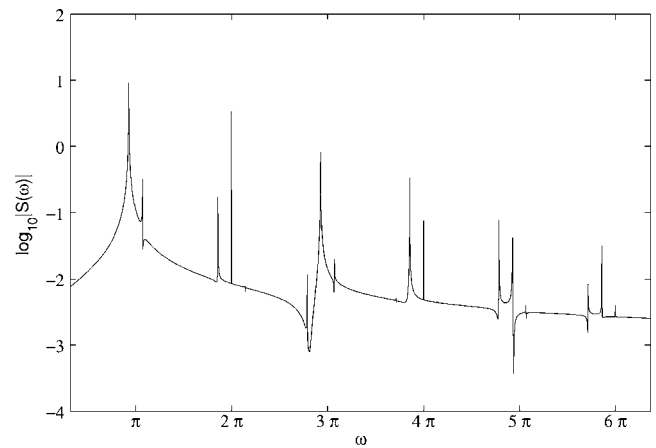

FIG. 8. Fourier spectrum of the ground state energy oscillations of the exciton energy (in units of E_∞) as a function of magnetic flux Φ_1/Φ_0 for $\Delta r = 0.7$ (in units of the reticular distance d_1) and $M = 5$ ($\rho_1 \sim 5.34$). $\gamma = 2.5$, $\epsilon = 1$, $\mu = 0.2$, and $N = 2$. Note that resonances at the frequencies $\omega_1 = 2\pi$ correspond to AB oscillations in the inner ring, and at $\omega_2 = 2.9$ correspond to oscillations due to nonbound components in different rings (as well as their harmonics). All logarithms are common (base 10) logarithms.

tween different rings, as shown in Fig. 9, an approximately exponential decay due to the AB effect can be detected, when the hopping between different rings and the diameter of the ring are small. In this case, the typical decay length is similar to the 1D equivalent case. The most interesting situation occurs when the hopping coefficient between different rings is similar to the hopping coefficient along the inner ring. If the circumference of the ring is small enough, AB oscillations are significant and they decay with the radius of the ring. Additionally, long–time oscillations appear whose amplitudes *increases* slightly with the circumference (and
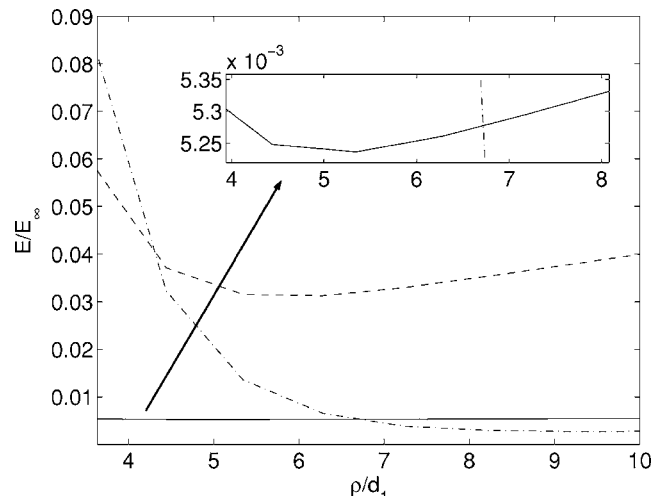

FIG. 9. Amplitude of the ground state energy oscillations (in units of E_∞) as a function of the circumference of the ring ρ (in units of circumferential lattice spacing d), corresponding to different values of distance between rings $\Delta r = 0.1$ (solid line), $\Delta r = 0.7$ (dashed line), and $\Delta r = 1.5$ (dot-dashed line). $\gamma = 2.5$ $\epsilon = 1$, $\mu = 0.2$, and $N = 2$. The arrow indicates the region which has been shown in more detail in the inset.
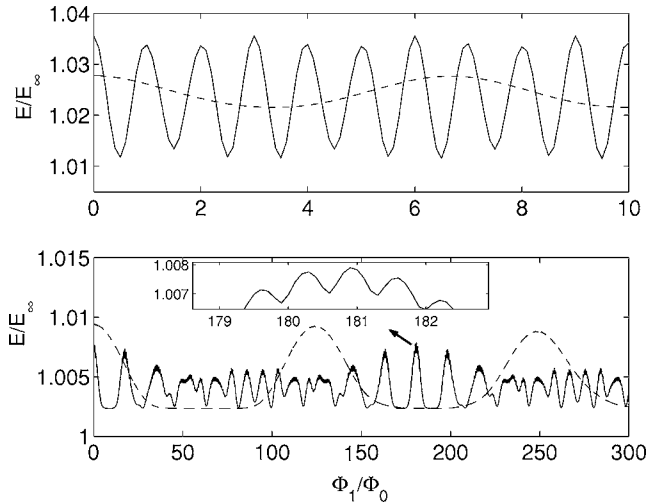
FIG. 10. Aharonov-Bohm oscillations of the exciton energy (in units of E_∞) as a function of Φ_1/Φ_0 for $N=5$ rings and several values of the distance between different rings $\Delta r = r_{i+1} - r_i$ and different values of the circumference of the inner ring ρ_1. $\gamma = 2.5$, $d_1 = 1$, $\epsilon = 1$, $\mu = 0.2$, and $k = 0$. $\Delta r = 1.5 d_1$ (top) and $\Delta r = 0.1 d_1$ (bottom). Continuous lines correspond to $M=5$ ($\rho_1 = 5.34$) and dashed lines to $M=13$ ($\rho_1 = 13.12$).

thus the enclosed flux) of the ring. This leads to the non-monotonicity observed in Fig. 9.

V. GENERAL CASE OF N ANNULAR RINGS

For arbitrary values of M and N, we have not been able to find a general expression for the Hamiltonian matrix. Nevertheless, if M and N are small enough, it is possible to calculate the eigenvalues and eigenvectors by using algebraic manipulation methods to construct an exact Hamiltonian matrix in algebraic form and then use a numerical eigenvalue solver for each parameter value.

As shown in Fig. 10, we have found essentially the same phenomena as in the previous section. If the distance between the rings is large enough, we can find AB oscillations due to the existence of components corresponding to non-bound states where the two fermions are in the inner ring. These oscillations decrease very rapidly when the circumference of the rings increases. When the distance between rings is small enough, there are also significant long-period oscillations due to the contribution of states corresponding to electrons and holes located in neighboring sites on different rings.

If we study the amplitude of the ground state energy oscillations as a function of the number of rings N as shown in Fig. 11, we can observe that there exists a weak dependence with the number of rings, but this dependence becomes negligible when N is more than a certain N_c, which in turn is a function of Δr. If Δr is large enough, $N_c \approx 1$. This suggests that, except when the distance between rings is very small, the dependence of the energy of the ground state with magnetic field is essentially a 1D phenomenon.

VI. A SYSTEM OF STACKED RINGS

In the case of a *stacked* array of rings with *identical* radius located along the magnetic field direction—and thus all
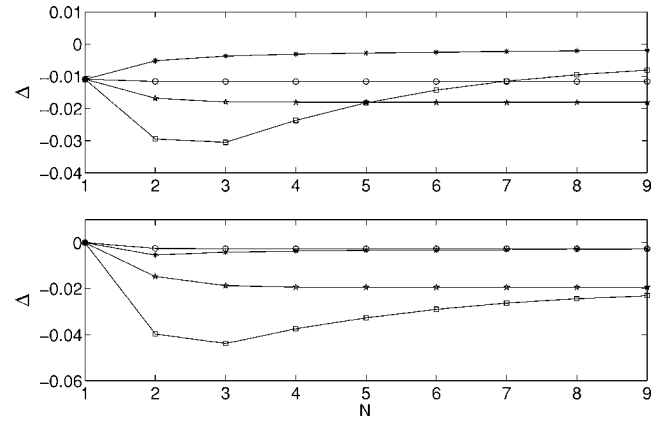

FIG. 11. Oscillations of the energy of the ground state as functions of the number of rings N. $\Delta = (E_{mx} - E_{min})/(2E)$, where E is the exciton energy for $B=0$. $f=5$, corresponding to $\rho_1 = 5.34$ (top), and $f=11$, corresponding to $\rho_1 = 11.15$ (bottom). ($*$) $\Delta r = 0.1$, ($\square$) $\Delta r = 0.7$, ($\star$) $\Delta r = 1.0$, and ($\bigcirc$) $\Delta r = 1.5$. $\gamma = 2.5$, $d_1 = 1$, $\epsilon = 1$, and $\mu = 0.2$.

of them threaded by the same magnetic flux—our results are similar to the single ring case. Only the oscillations of period $T = \Phi_1/\Phi_0$ are observed. If we further analyze the decay of the ΔE oscillations with the circumference of the rings, we find that it is nearly exponential and the decay length can be studied. As expected, if Δr is large, the stack behavior is similar to isolated rings. But if the rings are close, the decay length *increases* as shown in Fig. 12. This suggests that the bound exciton states use the additional rings as further channels along which to tunnel when prompted by the increasing magnetic flux.

VII. CONCLUSIONS

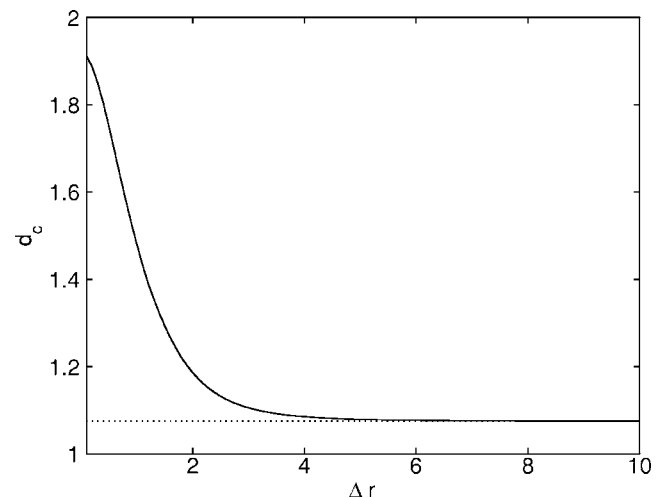In this paper we have studied the existence of AB oscillations for an exciton in a class of 2D annular models de-

FIG. 12. Decay length as a function of the distance between rings corresponding to two stacked rings (continuous line) for $\gamma = 2.5$ and reticular distance $d=1$. The dotted line corresponds to the 1D ring and has been calculated using Eq. (12).

scribed by an attractive fermionic Hubbard model. In all models, when the ring separation becomes small, the 1D continuum results can be recovered in a limit, and the structure of exact and approximate equations for the AB oscillations in the discrete lattice model is similar to those for the continuum model.

Our results for the vertically stacked ring system show that the addition of further transport channels leads to an increase of the decay length for the AB oscillations in the ground state. This effect indicates a route to enhancing the possibility of experimentally verifying the excitonic AB effect.

On the other hand, when additional transport channels are added in-plane to give a disc-shaped, multi-ring structure as studied in Secs. III–V, the excitonic AB oscillations are quickly lost in the oscillations which are due to the various additional flux periodicities in each ring. Already for the two-ring case, our results show quite complicated oscillation structures. Nevertheless, even in the general case studied in Sec. V, remnants of the original AB oscillations survive. These can be seen best when analyzing the Fourier spectrum.

ACKNOWLEDGMENTS

APPENDIX: EIGENVALUES AND EIGENVECTORS IN A 1D RING

We look for eigenvalues and eigenvectors of the matrix given by Eq. (4). The corresponding eigenvalue equation is

$$\hat{H}|\psi\rangle = E|\psi\rangle, \tag{A1}$$

where $|\psi\rangle \equiv (\psi_0, \psi_1, \dots, \psi_{M-1})^T \equiv \sum_{m=0}^{M-1} \psi_m |m\rangle$ with suitable (i.e., normalized, complete and orthogonal) atomic wave functions at each site m. Due to the special circulant form of

Eq. (4) (up to the modified corner element γ) we may consider $|\psi\rangle$ as being M periodic, that is, $\psi_{m+M} = \psi_m$.

1. Eigenvectors and eigenvalues

The system of equations generated by Eq. (A1) is

$$\gamma\psi_0 + q^*\psi_1 + q\psi_{M-1} = -E\,\psi_0 \tag{A2}$$

and

$$q\psi_{m-1} + q^*\psi_{m+1} = -E\,\psi_m, \tag{A3}$$

with $m \in \{1, \dots, M-1\}$ with periodic boundary conditions $\psi_{m+M} = \psi_m$. In addition, we choose the phase of ψ_0 to be zero, that is, $\psi_0 \in \mathbb{R}$. This fixes the overall phase factor up to which an eigenvector can be determined. We now solve the difference equation (A3). Its characteristic equation reads

$$q^*r^2 + Er + q = 0, \tag{A4}$$

whose solutions are

$$r_\pm = (\varepsilon \pm \sqrt{\varepsilon^2 - 1})e^{i\theta} = e^{i(\theta \pm \nu)}, \tag{A5}$$

where we have defined

$$q = |q|e^{i\theta}; \quad \varepsilon = -\frac{E}{2|q|} := \cos\nu. \tag{A6}$$

Note that if $|\varepsilon| > 1$, ν becomes purely imaginary. We can now write the solution of Eq. (A3) as

$$\psi_m = [A\cos(\nu M) + B\sin(\nu m)]e^{im\theta}. \tag{A7}$$

It is obvious that $A = \psi_0$ in the equation above and, using the periodicity condition $\psi_0 = \psi_M$

$$B = \frac{\psi_0}{\sin(\nu M)}[e^{-iM\theta} - \cos(\nu M)]. \tag{A8}$$

Thus

$$\psi_m = \frac{\psi_0}{\sin(\nu M)}\{e^{im\theta}\sin[(M-m)\nu] + e^{-i(M-m)\theta}\sin(\nu m)\}. \tag{A9}$$

With the convention that $\psi_0 \in \mathbb{R}$, we obtain from the latter equation that $\psi_{M-m} = \psi_m^*$. The normalization factor ψ_0 can be calculated exactly and reads

$$\psi_0 = \frac{\sin M\nu}{\left[M - \dfrac{\sin M\nu \cos M\nu}{\tan\nu} + \cos M\theta\left(\dfrac{\sin M\nu}{\tan\nu} - M\cos M\nu\right)\right]^{1/2}}. \tag{A10}$$

We now turn to the determination of the spectrum. Eigenvectors of Eq. (4) have to verify the "boundary condition" (A2). Using the general expression derived in Eq. (A9), this additional constraint results in

$$\frac{\tan(M\nu)}{\sin\nu} = \frac{2|q|}{\gamma}\left(1 - \frac{\cos(M\theta)}{\cos(M\nu)}\right). \tag{A11}$$

Given that $\hat{H}$ is Hermitian, its eigenvalues are real. As we have defined $E=-2|q|\cos \nu$, we see that Eq. (A11) has to be solved for $\nu \in \mathbb{R}$, $\nu \in i\mathbb{R}$, or $\nu \in \pi+i\mathbb{R}$ (the only distinct possibilities for E to be real). The solutions on the real axis ($\nu \in \mathbb{R}$) represent extended states whereas the unique solution on the imaginary axis ($\nu \in i\mathbb{R}$ or $\nu \in \pi+i\mathbb{R}$), if it exists, represents the bound state. Once Eq. (A11) has been solved for ν, the spectrum is obtained from $E=-2|q|\cos \nu$.

2. Existence of a bound state

We restrict hereafter to positive values of γ. It is obvious that the case $\gamma<0$ can be handled from the latter as $\hat{H}(-\gamma,q)=-\hat{H}(\gamma,e^{i\pi}q)$. For $\gamma>0$ the eigenvector equation is obtained from Eq. (A11) with $\nu=i\eta$, $\eta \in \mathbb{R}$. Then, Eq. (A11) reads

$$\frac{\tanh(M\eta)}{\sinh \eta} = \frac{2|q|}{\gamma}\left(1 - \frac{\cos(M\theta)}{\cosh(M\eta)}\right). \tag{A12}$$

A necessary and sufficient condition for a bound state to exist is given by Eq. (11). To prove the result we first rewrite (A12) as $f(\eta)=2|q|/\gamma$ where

$$f(\eta) = \frac{\sinh M\eta}{\sinh \eta(\cosh M\eta - \cos M\theta)}.$$

Differentiating f with respect to η we can show that, for $M \geq 1$ and $\eta>0$, $f'(\eta)<0$.

Now, $\lim_{\eta \to 0} f(\eta)=M/(1-\cos M\eta)$ and $\lim_{\eta \to \infty} f(\eta)=0$. Therefore, the solution of $f(\eta)=2|q|/\gamma$ exists if $2|q|/\gamma \leq M/(1-\cos M\eta)$, which establishes the result.

Note that when $\gamma=2|q|/M(1-\cos M\theta)$, the solution of Eq. (A12) is $\eta=0$. Then $\nu=0$ and Eq. (A9) shows that the bound state is not exponentially localized because $\psi_m \propto e^{in\theta}(M-m+me^{-iM\theta})$. This limiting case cannot really be considered a bound state, hence the strict inequality in Eq. (11).

3. Approximation for large (but finite) number of sites M

In this case it is possible to derive explicit approximate expressions for the eigenvalues both for extended and bound states.

a. Extended states ($\nu \in \mathbb{R}$)

Let us rewrite Eq. (A11) in the following form,

$$\sin[M\nu - \varphi(\nu)] = -\sin \varphi(\nu)\cos(M\theta), \tag{A13}$$

where $\tan \varphi(\nu)=2|q|\sin \nu/\gamma$. We can restrict our investigation to the interval $\nu \in [0,\pi)$ within which we will find M

-1 eigenvalues or M according to whether the condition (11) for the existence of a bound state is satisfied or not. If M is large, $\varphi(\nu)$ varies slowly as compared to $M\nu$ and the zeroth-order approximate solution for Eq. (A13) is

$$\nu_l^{(0)} = \frac{l\pi}{M}, \quad l \in \{0,\ldots,M-1\}. \tag{A14}$$

Let us seek an approximate solution of the form $\nu_l=\nu_l^{(0)}+\nu_l^{(1)}$. Then the first correction is given by

$$\nu_l^{(1)} = \frac{1}{M}\{\varphi(\nu_l^{(0)}) + \arcsin[(-1)^{l+1} \sin \varphi(\nu_l^{(0)})\cos(M\theta)]\}. \tag{A15}$$

b. Bound state ($\nu \in i\mathbb{R}$)

In this case, let $\nu=i\eta$. Then Eq. (A11) is given by Eq. (10). As $M\to\infty$, a first solution is

$$\eta^{(0)} = \text{arcsinh}\left(\frac{\gamma}{2|q|}\right), \tag{A16}$$

and the corresponding energy is

$$E^{(0)} = -2|q|\cos \nu = -2|q|\cosh \eta^{(0)} = -\sqrt{4|q|^2 + \gamma^2}, \tag{A17}$$

the solution for an infinite lattice. Notice that this value no longer depends on θ (i.e., the magnetic field). We can now use this last value to solve Eq. (A12) by a first Newton iteration, for instance

$$\eta \simeq \eta^{(0)} + \eta^{(1)}, \tag{A18}$$

where $\eta^{(1)}=-f(\eta^{(0)})/f'(\eta^{(0)})$ with

$$f(x) = \frac{\tanh(Mx)}{\sinh x} - \frac{2|q|}{\gamma}\left(1 - \frac{\cos(M\theta)}{\cosh(Mx)}\right). \tag{A19}$$

As $\eta^{(1)} \simeq -2\tanh \eta^{(0)} \cos(M\theta)e^{-M\eta^{(0)}}$, we finally obtain

$$\begin{aligned}
E &= -2|q|\cosh \eta \\
&\simeq -2|q|\cosh \eta^{(0)}[1 + 2\tanh 2\eta^{(0)} \cos(M\theta)e^{-M\eta^{(0)}}] \\
&= -\sqrt{4|q|^2 + \gamma^2}\left[1 + \frac{2\gamma^2}{4|q|^2 + \gamma^2}\right. \\
&\quad \left.\times\cos(M\theta)\exp -M \,\text{arcsinh}\left(\frac{\gamma}{2|q|}\right)\right].
\end{aligned} \tag{A20}$$

The factor containing the magnetic field through $\cos(M\theta)$ decreases exponentially with the number of sites M, that is with the radius of the ring (the lattice spacing is assumed to be constant).

*Corresponding author. Electronic address: palmero@us.es

†Current address: College of Engineering, Boston University, 44 Cummington Street, Boston, MA 02215.

[1] A. Lorke, R. J. Luyken, A. O. Govorov, J. P. Kotthaus, J. M. Garcia, and P. M. Petroff, Phys. Rev. Lett. **84**, 2223 (2000).

[2] A. Emperador, M. Pi, M. Barranco, and A. Lorke, Phys. Rev. B **62**, 4573 (2000).

[3] A. Lorke, R. J. Luyken, M. Fricke, J. P. Kotthaus, G. Medeiros-Ribeiro, J. M. Garcia, and P. M. Petroff, Microelectron. Eng. **47**, 95 (1999).

[4] M. Bayer, O. Stern, P. Hawrylak, S. Safard, and A. Forchel, Nature (London) **405**, 923 (2000).

[5] M. Bayer, M. Korkusinski, P. Hawrylak, T. Gutbrod, M. Michel, and A. Forchel, Phys. Rev. Lett. **90**, 186801 (2003).

[6] K. S. Cho, D. V. Talapin, W. Gaschler, and C. B. Murray, J. Am. Chem. Soc. **127**, 7140 (2005).

[7] Y. Aharonov and D. Bohm, Phys. Rev. **115**, 485 (1959).

[8] N. Byers and C. N. Yang, Phys. Rev. Lett. **7**, 46 (1961).

[9] R. A. Römer and M. E. Raikh, Phys. Rev. B **62**, 7045 (2000).

[10] A. V. Chaplik, Pis'ma Zh. Eksp. Teor. Fiz. **62**, 885 (1995) [JETP Lett. **62**, 900 (1995)].

[11] A. V. Chaplik and A. O. Govorov, Physica B **256–258**, 477 (1998).

[12] K. Maschke, T. Meier, P. Thomas, and S. W Koch, Eur. Phys. J. B **19**, 599 (2001).

[13] T. Meier, P. Thomas, and S. W. Koch, Eur. Phys. J. B **22**, 249 (2001).

[14] H. Hu, J. L. Zhu, D. J. Li, and J. J. Xiong, Phys. Rev. B **63**, 195307 (2001).

[15] A. V. Maslov and D. S Citrin, Phys. Rev. B **67**, 121304(R) (2003); A. Bruno-Alfonso and A. Latgé, *ibid.* **71**, 125312 (2005).

[16] E. H. Lieb and F. Y. Wu, Phys. Rev. Lett. **20**, 1445 (1968).

[17] A. C. Scott, *Nonlinear Science*, 2nd. ed. (Oxford University Press, Oxford, 2003).

[18] A. C. Scott, J. C. Eilbeck, and H. Gilhøjet, Physica D **78**, 194 (1994).

[19] V. Fleurov, Chaos **13**, 676 (2003); R. S. MacKay, Physica A **288**, 174 (2000).

[20] J. Dorignac, J. C. Eilbeck, M. Salerno, and A. C. Scott, Phys. Rev. Lett. **93**, 025504 (2004).

[21] J. C. Eilbeck and F. Palmero, in *Proceedings of the NATO ARW: Nonlinear Waves: Classical and Quantum Aspects* (Kluwer Academic Publishers, Dordrecht, Netherlands, 2004), p. 399.

[22] F. Fillaux and C. J. Carlile, Phys. Rev. B **42**, 5990 (1990); F. Fillaux, C. J. Carlile, and G. J. Kearley, *ibid.* **44**, 12280 (1991); **58**, 11416 (1998).

[23] T. Asano, H. Nojiri, Y. Inagaki, J. P. Boucher, T. Sakon, Y. Ajiro, and M. Motokawa, Phys. Rev. Lett. **84**, 5880 (2000).

[24] L. S. Schulman, E. Mihóková, A. Scardicchio, P. Facchi, M. Nikl, K. Polák, and B. Gaveau, Phys. Rev. Lett. **88**, 224101 (2002).

[25] F. Gebhard and A. E. Ruckenstein, Phys. Rev. Lett. **68**, 244 (1992).

[26] B. S. Shastry and B. Sutherland, Phys. Rev. Lett. **65**, 243 (1990).

[27] B. Sutherland and B. S. Shastry, Phys. Rev. Lett. **65**, 1833 (1990).

[28] F. Essler, H. Frahm, F. Göhmann, A. Klümper, and V. Korepin, *The One-Dimensional Hubbard Model* (Cambridge University Press, Cambridge, 2005).

[29] J. C. Eilbeck, in *Localization and Energy Transfer in Nonlinear Systems* (World Scientific, Singapore, 2003).

[30] F. Göhmann and V. E. Korepin, Phys. Lett. A **260**, 516 (1999).

[31] J. C. Eilbeck and F. Palmero, Phys. Lett. A **331**, 201 (2004).

[32] A. O. Govorov, S. E. Ulloa, K. Karrai, and R. J. Warburton, Phys. Rev. B **66**, 081309(R) (2002).